A Geometry-Based Stochastic Model for Truck Communication Channels in Freeway Scenarios

Chen Huang, *Member, IEEE*, Rui Wang, *Member, IEEE*, Cheng-Xiang Wang, *Fellow, IEEE*, Pan Tang, *Member, IEEE*, and Andreas F. Molisch, *Fellow, IEEE*

***Abstract*— Vehicle-to-vehicle (V2V) wireless communication systems are fundamental in many intelligent transportation applications, e.g., traffic load control, driverless vehicle, and collision avoidance. Hence, developing appropriate V2V communication systems and standardization require realistic V2V propagation channel models. However, most existing V2V channel modeling studies focus on car-to-car channels; only a few investigate truck-to-car (T2C) or truck-to-truck (T2T) channels. In this paper, a hybrid geometry-based stochastic model (GBSM) is proposed for T2X (T2C or T2T) channels in freeway environments. Next, we parameterize this GBSM from the extensive channel measurements. We extract the multipath components (MPCs) by using a joint maximum likelihood estimation (RiMAX) and then determine the cluster types based on their evolution patterns. We classify the determined clusters into line-of-sight, single-bounce reflections from static interaction objects (IOs), single-bounce reflections from mobile IOs, multiple-bounce reflections, and density multipath components (DMCs). Particularly, we model multiple-bounce reflections as double clusters following the COST 273/COST2100 method. This paper presents the complete parameterization of the channel model. We validate this model by comparing the delay spread and the angular spreads of arrival/departure obtained from the proposed model with the measurement data.**

***Index Terms*— GBSM, truck-to-truck communications, truck-to-car communications, channel measurements, channel parameter estimation.**

Manuscript received 28 October 2021; revised 14 April 2022; accepted 8 June 2022. Date of publication 20 June 2022; date of current version 16 August 2022. This work was supported by the National Key R&D Program of China under Grant 2018YFB1801101, the National Natural Science Foundation of China (NSFC) under Grant 61960206006, the High Level Innovation and Entrepreneurial Research Team Program in Jiangsu, the High Level Innovation and Entrepreneurial Talent Introduction Program in Jiangsu, the EU H2020 RISE TESTBED2 Project under Grant 872172, the China Postdoctoral Science Foundation under Grant 2021M702499, and the Outstanding Postdoctoral Fellow Program in Jiangsu. The work of Rui Wang and Andreas F. Molisch was supported by the California Transportation Authority/METRANS and by the National Science Foundation. The associate editor coordinating the review of this article and approving it for publication was I. Guvenc. *(Corresponding author: Cheng-Xiang Wang.)*

Chen Huang is with the Pervasive Communication Research Center, Purple Mountain Laboratories, Nanjing 211111, China, and also with the National Mobile Communications Research Laboratory, School of Information Science and Engineering, Southeast University, Nanjing 210096, China (e-mail: huangchen@pmlabs.com.cn).

Rui Wang was with the Ming Hsieh Department of Electrical and Computer Engineering, University of Southern California, Los Angeles, CA 90007 USA. He is now with Samsung Research America, Mountain View, CA 94043 USA (e-mail: rui1.w@samsung.com).

Cheng-Xiang Wang is with the National Mobile Communications Research Laboratory, School of Information Science and Engineering, Southeast University, Nanjing 210096, China, and also with the Pervasive Communication Research Center, Purple Mountain Laboratories, Nanjing 211111, China (e-mail: chxwang@seu.edu.cn).

Pan Tang is with the State Key Laboratory of Networking and Switching Technology, Beijing University of Posts and Telecommunications, Beijing 100876, China (e-mail: tangpan27@bupt.edu.cn).

Andreas F. Molisch is with the Ming Hsieh Department of Electrical and Computer Engineering, University of Southern California (USC), Los Angeles, CA 90089 USA (e-mail: molisch@usc.edu).

Color versions of one or more figures in this article are available at https://doi.org/10.1109/TCOMM.2022.3184344.

Digital Object Identifier 10.1109/TCOMM.2022.3184344

I. Introduction

INTELLIGENT transportation systems (ITSs) have drawn much attention and expectations from the transportation and wireless communication industries as ITS is a promising solution to traffic congestion and problems in street security [1], [2]. Accordingly, vehicle to vehicle (V2V) communications have been played a significant part for developing the ITS functionalities, e.g., traffic load control, driverless vehicles, and collision prevention. Therefore, V2V communications have received much attention from the academia and the industry, e.g., [4], [5]. Most of the related studies in this area focus on dedicated short-range communications system for ITSs, e.g., IEEE 802.11p [6] and IEEE 802.11bd [7]. V2V is also an important communication scenario for 5G and beyond 5G (B5G)/6G communications systems [8]–[10]. Therefore, numerous studies from both the 3GPP and the academia have explored the application of LTE or 5G-NR for V2V communications [11]. Particularly, the studies consider LTE-V and the 5G sidelink technology developed in 3GPP Release 16 as an alternative to the 802.11p/bd standards. Regardless of what technology will be ultimately chosen, V2V communications will be widely applied in the future to provide safe and trustworthy connections with short latency and high data speeds needed by ITSs.

The study of propagation channels is a fundamental aspect in any wireless communication system design, network optimization, and performance evaluation [12]. Therefore, to realize advanced ITS networks that meet the above requirements, the corresponding wireless channels need to be thoroughly studied. Compared to the usual cellular communication scenarios, the V2V channels, especially in the freeway scenario, have the following features [13]:

1) V2V channels are usually time-varying and nonstationary due to the movements of the receiver (Rx) and transmitter (Tx) vehicles.
2) The denseness and speed of vehicles (both Tx/Rx vehicles and other vehicles) strongly impact the nonstation-

ary nature of V2V channels; this state is much more pronounced in the freeway scenario than in other common scenarios.

3) The Tx and Rx are all placed at relatively low altitude (approximately 1–2 m for car-to-car (C2C), 1.5–2.5 m for T2X); thus, the changes in V2V channels are greater in the azimuth region than in the elevation region.
4) Due to the low altitude of the Tx/Rx and the environment (usually surrounded by other vehicles and buildings), the communication distance is relatively small (approximately 20–300 m).
5) Compared to other V2V scenarios, e.g., urban street canyons, the highway V2V scenario has more vehicles present in the environment, albeit it has fewer buildings around the Tx/Rx vehicles.

Several measurements under highway V2V scenarios have already been conducted owing to its special nature and importance in transportation communication. These studies include single-input single-output (SISO) channel measurements in the 2.4 GHz [14], 5 GHz [15], 5.2 GHz [16], [17], 5.9 GHz [18]–[26], and 59.6 GHz band [27]; multiple-input single-output channel measurements in the 5.75 GHz band [28]; and multiple-input multiple-output (MIMO) channel measurements in the 5.2 GHz [29]–[31], 5.3 GHz [32], [33], and 5.6 GHz band [34], [35]. However, the above papers focus on C2C communications; only a few channel measurements involved trucks. Furthermore, these measurements usually see trucks as obstacles: [26], [36]–[39] studied the obstructed fading of the truck, whereas [28], [40] mainly focused on the diffraction around a truck. Ref. [41] measured the SISO shadowing characteristics and delay spread in both urban and highway scenarios and viewed trucks as obstacles; likewise, the study did not measure multi-antenna characteristics. Ref. [42] conducted truck-to-truck (T2T) measurements in a truck platoon, but the results were restricted to pathloss and diversity gain. Research on truck-to-car (T2C) and T2T MIMO channel models (known as T2X channel model) is very limited despite being an important scenario, especially in a freeway environment. T2X channels behave differently from C2C due to the relatively higher height of trucks; thus, cars around the Tx/Rx are less likely to block the signal, thereby leading to greater reflection from the cars in different/opposite lanes.

Future measurements should then inform which channel models can be used for system design and simulations. Both 802.11bd and 5G-NR anticipated the use of MIMO transmission for this purpose as it is very suitable for satisfying the demands of low latency and high data speeds communications [43]. Thus, a channel model needs to be suitable for the MIMO system simulations. According to the modeling method, the existing channel models could be divided into different types: i) *deterministic channel models*, which determine the multipath components (MPCs) deterministically by using ray-tracing or ray-launching [44]; ii) *nongeometrical stochastic channel models* that characterize MPCs without having to consider any potential geometry, e.g., 3-D V2V models in [45] and the stochastic models in [15], [46]; and iii) geometry-based stochastic channel models (GBSMs) that model the interaction objects (IOs) in different random distributions and then adopt a simplified ray tracing to acquire the real impulse response. Specifically, it can be further separated into regular-shape GBSMs (RS-GBSMs), i.e., deploy the IOs in a regular-shape-like circles [47], ellipses [48], rings [49], or two cylinders model [50]; and *irregular-shape GBSMs* (IS-GBSMs), i.e., reconstruct a physical geometry map of the environment to model the position and distributions of the IOs in different scenarios [17], [51]–[54], [62].

IS-GBSMs inherently capture the characteristics of double-directional channel to analyze MIMO channels; thus, it naturally suits nonstationary environment [55], [56] and provide good agreement with measurements because they are parameterized from them. Furthermore, they could be readily extended to other scenarios by modifying the geometry map.

It has been found in numerous channel measurements that obtained MPCs are usually allocated in clusters [57]. Meanwhile, many well-known channel models and standards have been developed based on a cluster structure, e.g., the Saleh-Valenzuela model, COST 2100/259, and 3GPP Spatial Model. Using hybrid IS-GBSM is an efficient way of reproducing the cluster construction of channels. For example, COST 259 integrates the traditional GBSM and stochastic models by deciding intercluster parameters on the geometry map of environments and intracluster parameters on the statistic characteristics of channels. Because intracluster features are modeled as distributions with no geometric detailed information, the hybrid IS-GBSM is better than the traditional GBSM in realizing the trade-off between model intricacy and accuracy. However, most of the existing IS-GBSM [17], [51], [62] consider only the single bounce reflection during the propagation, which is not necessarily true according to the observations in [53].

In our previous work [53], we have proposed a geometrical cluster-based hybrid IS-GBSM for C2C communications in urban street canyon scenarios. In this paper, we expand our study to T2C and T2T communications in freeway scenarios. We parameterize the model based on the wide measurement activity conducted in the freeway circumstance in Los Angeles, CA, USA. The major contributions of this paper can be summed up as follows:

- We performed an extensive campaign to measure the MIMO propagation channels between T2C and T2T in a freeway environment.
- We obtain the MPC parameters through high-resolution algorithm; we then extract and characterize the clusters from the measurement data based on the cluster evolution pattern. By cross-checking the measurement video and the channel properties of each cluster, we classify all clusters into different types, including twin clusters, to model the multiple-bounce reflection, and thus make the model more accurate.
- We parameterize the model for both T2C and T2T channels and give a complete model parameter list.
- We validate the proposed parameterization by comparing the synthetic data generated by the proposed model to the measurement data collected from another part of the freeway. The data we use to verify our model were collected from a different part of the freeway, and we compare them

to the data utilized for the model parameterization. This shows that our own model can stand for typical freeway environments.

The rest of the paper is arranged as follows. Section II briefly describes the channel measurement campaign, which acts as the foundation for the parameterization and validation of the proposed GBSM. Section III introduces the general data processing progress, including the MPC parameters estimation, tracking, and clustering. Section IV describes the proposed model outline and details the general construction of the model. We also outline here the different type of clusters of the channel model and parameterize the clusters from the measurement. Section V compares the synthetic data generated by the channel models to the actual measurement data. And lastly, Section VI draws the conclusions.

II. A Truck-to-Truck/Car Measurement Campaign

This part presents the details of the conducted T2C and T2T MIMO channel measurement campaign. The proposed T2X channel model is developed based on this measurement campaign, i.e., we draw the parameters of our model from this measurement. To limit the scope, this paper gives only a brief introduction; [58] gives a more detailed introduction on the antenna arrays and the measurement.

A. Measurement Setup

We conducted the V2V measurement campaigns by using a self-built real-time MIMO channel sounder depicted in [58]. The system contains a pair of NI-USRP RIO, which we used as major radio frequency transceivers. The USRPs are linked to two eight-element uniform circular arrays (on both Tx and Rx side) through electronic switches.

A pair of eight-element uniform circular arrays were linked to the USRPs through electronic switches. The multitone waveform is selected to serve as a detection signal and was approximated at the Zadoff-Chu sequence. Each snapshot sample has a duration of $T_0 = 640\mu$s, which consisted (8×8) samples of detection signals (including protection periods), and is required in-between the samples to determine the time of the Tx and Rx switches. The transmission signals were done in bursts, consisting of 60 concatenated MIMO snapshots; thereafter, a dead time was inserted to allow the acquired data to stream into a local hard disk. The bursts were repeated every 100 ms. The Rx and Tx reference clocks were synchronized via a pair of GPS-disciplined Rb clocks, which synchronized the rates of recurrence and timing at the Rx and Tx.

The major system settings is given in Table I and Fig. 1 shows the measurement setup. Fig. 1(a) displays the vehicles used in the measurement: the red SUV was the Rx vehicle, whereas the white truck was the Tx vehicle (in the T2T measurements, two identical trucks were used for both Tx and Rx); Fig. 1(b) shows the antenna arrays on top of the vehicles. Note that the position of the antenna arrays on the vehicles and the shape of the vehicles can influence the communications channels. Specifically, we found that the container of the truck significantly impacts the communications channels, as detailed in the Section III.

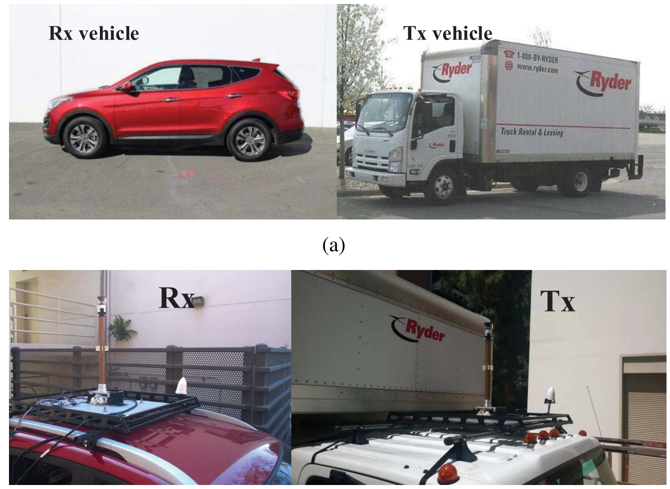

(a)

(b)

Fig. 1. Vehicles used in the measurement campaign. (a) used vehicles, i.e., the red SUV as the Rx vehicle, the white truck as the Tx vehicle; (b) antenna arrays on top of the vehicles.

TABLE I
System Setup of the T2X Measurement Campaign

Parameter	Value
Number of Rx antennas	8
Number of Tx antennas	8
Number of frequency tones	61
Number of MIMO per burst	60
Transmit power	26 dBm
Bandwidth	15 MHz
Carrier frequency	5.9 GHz
Length of the sounding signal	4 μs
Sampling rate	20 MS/s
MIMO signal duration	620 μs

B. Measurement Environment and Road Traffic

We conducted the channel measurement along the I-10 freeway in Los Angeles, USA. Each major lane of the highway consists of five lanes, with scattered buildings and vegetation on every side of the highway. The external border of the street is protected by sound barriers or concrete walls. The two major lanes of the highway are divided by a 0.50-meter-tall metallic rail. The Rx and Tx vehicles were traveling at the velocity of 20–30 m/s in actual traffic conditions (light to heavy traffic, etc.). Note that these conditions are not typical in Los Angeles, where the stop-and-go type of traffic is more common. However, the flowing traffic present during our measurements is typical in highway environments. Fig. 2(a) gives the scenario information of the measurement campaign. The red solid line, i.e., *Part I*, represents the part of the highway where we collected the data for the model parameterization. The blue dashed line, i.e., *Part II*, represents the stretch of highway where the data for the model verification were collected. We put panoramic cameras near the Rx and Tx to help us record the environment during the entire duration of the measurement. Figs. 2(b) and (c) are the recorded snapshots in the video from the Tx truck for the T2C and T2T, respectively.

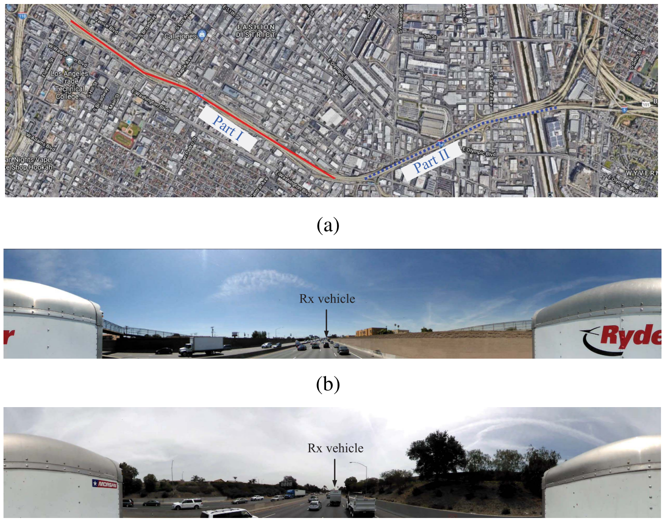

(a)

(b)

(c)

Fig. 2. Measurement environment. The red solid line and the blue dashed line in (a) represent the roads where we collected the data for the model parameterization and model verification, respectively; (b) and (c) are snapshots of the video recorded from the Tx side for T2C and T2T, respectively.

The video was used to help replicate the propagation environment, distinguish different clusters, and calibrate the position and speed of the Rx and Tx provided by the GPS estimations. For detailed information, see Sections III and IV.

III. Measurement Data Processing

A. Estimation of MPC Parameters

Similar to our previous C2C channel modeling work in [53], an effective and accurate iterative maximum likelihood estimation (MLE) process, i.e., the joint maximum likelihood estimation (RiMAX), is conducted to extract the MPCs. RiMAX can perform a joint MLE of these entire set of specular path (SP) parameters. In particular, the method can converge considerably quicker than the commonly used space alternating generalized expectation-maximization [59] algorithm, as used in [45], to estimate the MPCs from the V2V channel measurements. Furthermore, dense multipath components (DMCs) is also considered in the RIMAX method, which is a significant part in V2V channels. Note that, there are mainly two major differences between our implementation in [60] and the conventional RIMAX procedure [61]: i) the SP signal data model contains a phase shift in the antennas when it switches to another antenna elements; ii) new obtained path is only identified at the end of the MIMO snapshot rather than at the beginning. To reconstruct fast time-varying channels, it requires further pre-define the whole parameter vector model before extracting the new SPs. Therefore, the signal model is given as

$$H(t) = H_{\rm sp}(t) + H_{\rm dmc}(t) + n(t) \tag{1}$$

where $H_{\rm dmc}(t)$ and $n(t)$ denote the DMCs and the noise, respectively. Particularly, the DMCs are modeled, according to [61], as zero mean complex Gaussian distributions, whereas noise is considered as the white Gaussian noise. The SPs in (1) is further modeled as

$$H_{\rm sp}(f,t) = \sum_{l=1}^{L} b_{\rm R}(\Omega_{{\rm R},l}) b_{\rm T}^{T}(\Omega_{{\rm T},l}) \cdot r_l e^{-j(2\pi f \tau_l - \nu_l t)} \tag{2}$$

where $b_{\rm R}(\Omega_{\rm R})$ is the Rx antenna response at the azimuth domain, whereas $b_{\rm T}(\Omega_{\rm T})$ is the Tx antenna response at the azimuth domain. The notations r_l, τ_l, and ν_l are the weight factor, the path delay, and the Doppler of the lth path, respectively. The detailed information of conducted RIMAX procedure is given in [60].

Considering that most of the IOs in the freeway scenario are distributed at a similar height as those of the Rx/Tx vehicles, e.g., [45], a pair of uniform circular arrays is used at both the Rx and Tx sides. Our study thus concentrates on the azimuth domain, with the azimuth of arrival (AoA) and the azimuth of departure (AoD) angles ranging within $[-180°, 180°]$.

From the extraction results, we find that each MPC with AoD within the range of $[-90°, 90°]$ is repeated within (as reflected on) the range of $[-180°, -90°]$ and $[90°, 180°]$, which is mainly due to the mirror reflection of the container of the truck. For example, Fig. 3 plots the line-of-sight (LoS) MPCs in T2C channels with AoD at around $[-50°, 50°]$, and the "mirror MPC" of the LoS with AoD at around $[125°, 180°]$ and $[-180°, 140°]$. Every solid dot stands for an extracted MPC, the color stand for the MPCs' power (in dB), whereas the dots' size represents the delay (bigger size indicates lower delay). Note that, the data in Fig. 3 is specifically collected in an open area to verifying the "mirror MPCs". Both T2C and T2T channels exhibit this "mirror MPC" of the LoS since similar trucks were used.[1] The "mirror MPCs" are caused by the reflection of the container; thus, they do not contain information about the interaction of the objects behind the truck, e.g., cars or buildings, but repeat only the MPCs within $[-90°, 90°]$. Therefore, to simplify the model, we process only those MPCs with AoD and AoA within the range of $[-90°, 90°]$ and $[-180°, 180°]$, respectively, for the T2C channel data and those MPCs with AoD and AoA within the range of $[-90°, 90°]$ and $[-90°, 90°]$, respectively, for T2T channel data.

Fig. 4 displays the MPCs' evolution in the AoA domain over time. Fig. 4(a) is collected from T2C channels and Fig. 4(b) is collected from T2T channels. Specifically, Fig. 4(a) shows a large number of MPCs (in addition to those MPCs that change angles and appear/disappear similar to the NLOS case discussed below) that can be constantly observed in consecutive snapshots, with AoA at around $+/-180°$ (corresponding to the back of the Rx vehicle, as the coordinate displayed in Fig. 2(b)). Those MPCs belong to the LoS or the ground reflection (which are hard to be distinguished from the LoS part [53], [62], [63]), considering the geometrical relationship between the location of Tx and Rx.

On the other hand, Fig. 4(b) shows no such LoS MPCs. This is consistent with the physical environment where the container of the truck blocks the LoS, as shown in the truck antennas in Fig. 1(b) and the video sample in Fig. 2(b).

[1] This is a common setting for the truck antenna. However, using a different truck model may lead to different propagation environments.

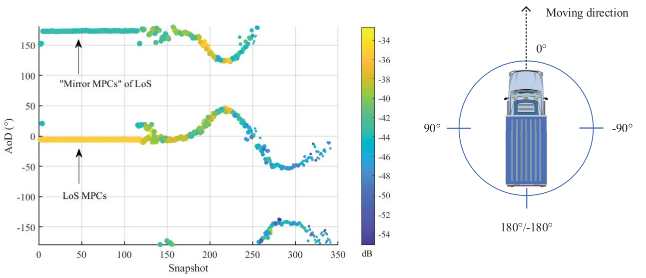

(a) (b)

Fig. 3. Illustration of the mirror reflection of the container of the truck: (a) the LoS and "mirror MPCs" of the LoS in T2C channels; (b) the coordinates of the Tx/Rx vehicle.

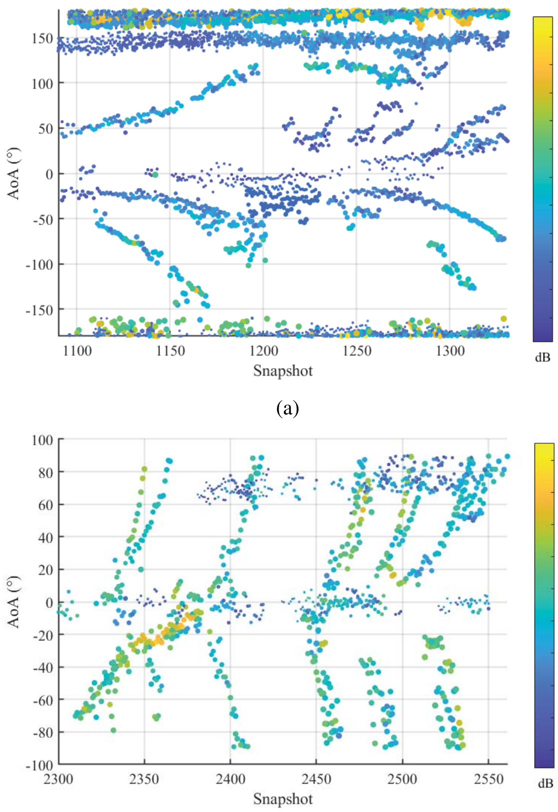

(a)

(b)

Fig. 4. Extracted MPCs by using RIMAX in [60]. (a) MPCs from T2C channels; (b) MPCs from T2T channels.

In addition, numerous MPCs come from different angles and show clear evolution patterns, which might be due to the reflections of the local IOs, e.g., other cars and buildings near or going toward the Rx and Tx vehicles. Specifically, the average coherence time of the T2C channels is approximately 0.06s, whereas the average coherence time of the T2T is approximately 0.007s. Since the T2T channels are NLoS channels whereas the T2C channels are LoS channels, the T2C channels thus have relatively larger average coherence time. The coherence time is related to the Doppler spread of the clusters, a smaller coherence time indicates to a bigger Doppler spread of the clusters, which is usually caused by a higher moving speed of the corresponding scatterers (relative to the Tx/Rx), and ultimately leads to stronger evolution of the dynamic clusters.

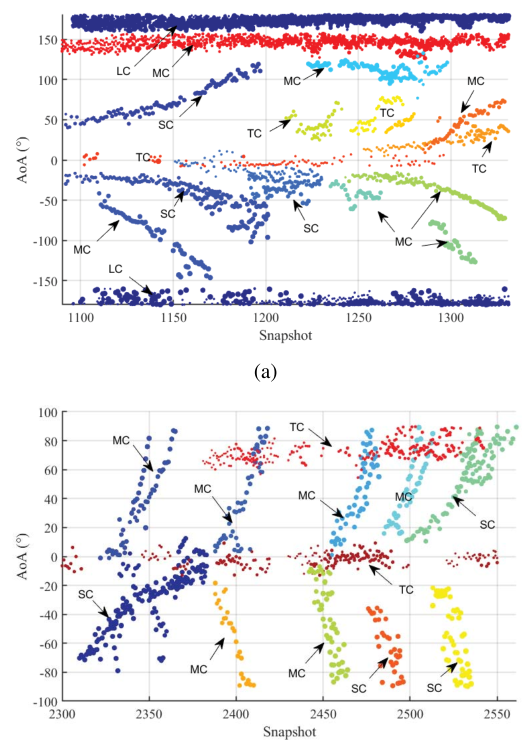

(a)

(b)

Fig. 5. Samples of cluster identification results for MPCs, where the four types of the clusters, i.e., LOSC, MC, SC, and TC, are labeled. (a) T2C channels and (b) T2T channels.

B. Cluster Identification

As briefly discussed in Section I, a cluster-based model can determine a good trade-off between model complexity and model accuracy; thus, we apply such approach to our model. We can see in Fig. 4 that the MPCs are distributed in groups/clusters, which show obvious similarity in the evolution pattern over time—they correspond to the (relative) moving pattern of the IOs in the environment. Therefore, these evolving clusters can be recognized by tracking and by clustering the MPC parameter estimation results in consecutive snapshots. Several cluster identification algorithms have been proposed for time-varying V2V channels, e.g., [64]–[68]. In this work, we adopt the tracking joint clustering algorithm [68] to identify the clusters based on their own evolution patterns over time, which is inherently suitable for our problem. To limit the range of this paper, we concentrate on the modeling procedure. Ref. [68] provides a more detailed information about the clustering procedure.

Fig. 5 offers a case of time-varying cluster identification outcomes for MPCs in (a) T2C channels and (b) T2T channels by using the algorithm in [68]. In Fig. 5, the different colors stand for the different cluster IDs. The geometry cluster-based model is built based on the different types of clusters caused by different types of IOs; thus, we categorize the clusters into the following four types:

- *LoS cluster* (LC): mainly composed of LoS MPCs and unresolvable ground reflections;

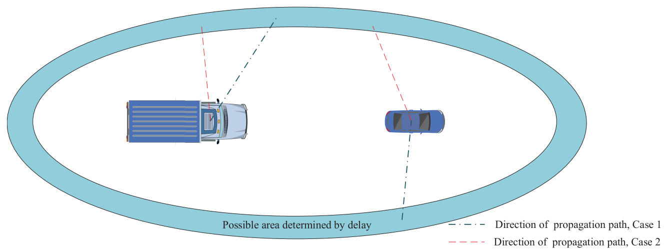

Fig. 6. Illustration of the TC extraction principle. Generally, the MPCs are determined as multiple bounce component if the lines connecting the AoA and AoD do not intersect at a point that lies on the ellipse that corresponds to the delay.

- *Mobile cluster* (MC): mostly composed of single-bounce reflections from mobile IOs, e.g., moving cars on the road;
- *Static cluster* (SC): mostly composed of single-bounce reflections from static IOs, e.g., buildings on the side of the road; and
- *Twin cluster* (TC): mostly composed of the multi-bounce reflection from any IOs.

Example of identified four types clusters are labeled in Fig. 5 as well.

In the RiMAX, the DMC is modeled as single exponential decay construction (rather than as clusters) and are uniform in the azimuth.

We identify the category of each cluster based on the measurement video and by cross-checking the AoA, AoD, and delay of each cluster. In single-bounce reflections, the lines connecting the AoA and AoD must intersect at a point that lies on the ellipse that corresponds to the delay, i.e., the blue area in Fig. 6. Specifically, if an MPC's AoD, AoA, and the delay cannot be consistent within a single-bounce reflection progress geometrically, it will be identified as a multi-bounce path. For example, a component departing from one side of the street and arriving at another side of the street is clearly multi-bounce, i.e., case 1 in Fig. 6. In another word, the AoA and AoD of the MPC show the opposite signs. Moreover, to ensure accuracy, all extracted TCs are verified through visual inspection according to the measurement video. In multi-bounce reflections, on the other hand, the detailed propagation progress is difficult to determine because the IOs are unknown, except for the one causing the first and the last reflection. Moreover, it is even harder to determine how many bounces have happened during the propagation. Hence, we use the *twin cluster* approach introduced in [69] and also adopted in the COST 273 and COST 2100 [72]. In this model, the first and last IOs in the propagation progress are modeled without considering the specific propagation details between these two IOs and uses the excess delay as the pseudo-distance between the first IOs and the last IOs.

Based on the identified and categorized clusters, a GBSM is presented in the following section.

IV. GBSM FOR T2X

This part introduces the GBSM for T2X channels. We first elaborate the model framework, then detail how the model parameters are extracted, and present tables containing the whole set of model parameters.

A. General Model Framework

The general model outline is consistent with our C2C model for the street canyon in [53]. The key idea in [53] is to set different types of IOs by using different stochastic distributions, set different channel characteristics to the reflected clusters from these IOs, then calculate the corresponding signal contributions based on the generated clusters, and finally fully sum all the signal contributions up. To achieve that, we reconstruct the geometrical map according to the physical setting of the measurement campaign, as illustrated in Fig. 7. Specifically, the notation W_{lane} is the width of each lane in freeway and $W_{\text{buildings}}$ is the width of the building area on the two sides of the street. The IOs in Fig. 7 are further categorized into two types: mobile IOs, e.g, moving cars in the street; and static IOs, e.g., the architectures on both sides of the road. In the model, all static IOs (buildings) are randomly distributed in the building area, with coordinates $\{x_{s_i}, y_{s_i}\}$, The details are provided in the Section IV-B.

The measurement campaign has the Rx car, with coordinates $\{x_{\text{R}}(t), y_{\text{R}}(t)\}$, running in front of the Tx truck, with coordinates $\{x_{\text{T}}(t), y_{\text{T}}(t)\}$. The Rx car and the Tx truck are traveling along the road with length L_{Length}, where the v_{R} and v_{T} are the moving velocities of the Rx car and Tx truck, respectively. The vehicles in the other lanes are moving around the Rx car and the Tx truck at coordinates $\{x_{m_i}(t), y_{m_i}(t)\}$ and velocity of v_{m_i}, where i is the index of other vehicles. Note that the speed of the Tx/Rx and that of each vehicle can be set to a different value in accordance with the physical environment.

In our work, the reflected paths caused by each IO are modeled as independent dynamic (time-varying) clusters, which have different channel characteristics, i.e., AoD/AoA, delay, intracluster delay/angular spread as well as the number of cluster members. As described in (1), the signal model is divided into two components: SPs and DMCs. Such that, the time-varying double-directional channel response of SPs, h_{sp} is modeled as the sum of all MPCs in all clusters, as given as

$$\begin{aligned} h_{\text{sp}}(t, \tau, \Omega_R, \Omega_T) = & \sum_{n=1}^{N} \sum_{l=1}^{L_n} \alpha_{n,l} e^{j\chi_{n,l}} \times \delta(\tau - \Delta\tau_{n,l} - T_n) \\ & \times \delta(\Omega_R - \Delta\omega_{R,n,l} - \Omega_{R,n}) \\ & \times \delta(\Omega_T - \Delta\omega_{T,n,l} - \Omega_{T,n}) \end{aligned} \tag{3}$$

where N is the total number of the cluster and L_n is the number of MPCs in the nth cluster, T_n is the delay of the nth cluster-center, $\Omega_{R,n}$ and $\Omega_{T,n}$ are the AoA and AoD of the nth cluster-center, respectively. For the nth cluster, $\Delta\tau_{n,l}$ is the delay of the lth MPC with respect to the cluster center, whereas the $\Delta\omega_{R,n,l}$, $\Delta\omega_{T,n,l}$ are the AoA and AoD of the lth MPC with respect to the cluster center, $\alpha_{n,l}$ is the complex amplitude of the lth MPC inside the nth cluster, $e^{j\chi_{n,l}}$ is path phase, and $\delta(\cdot)$ represents the Dirac delta function. The coefficient $\chi_{n,l}$ is modeled by using stochastic variables, which is equally allocated over $[0, 2\pi)$. Note that this part

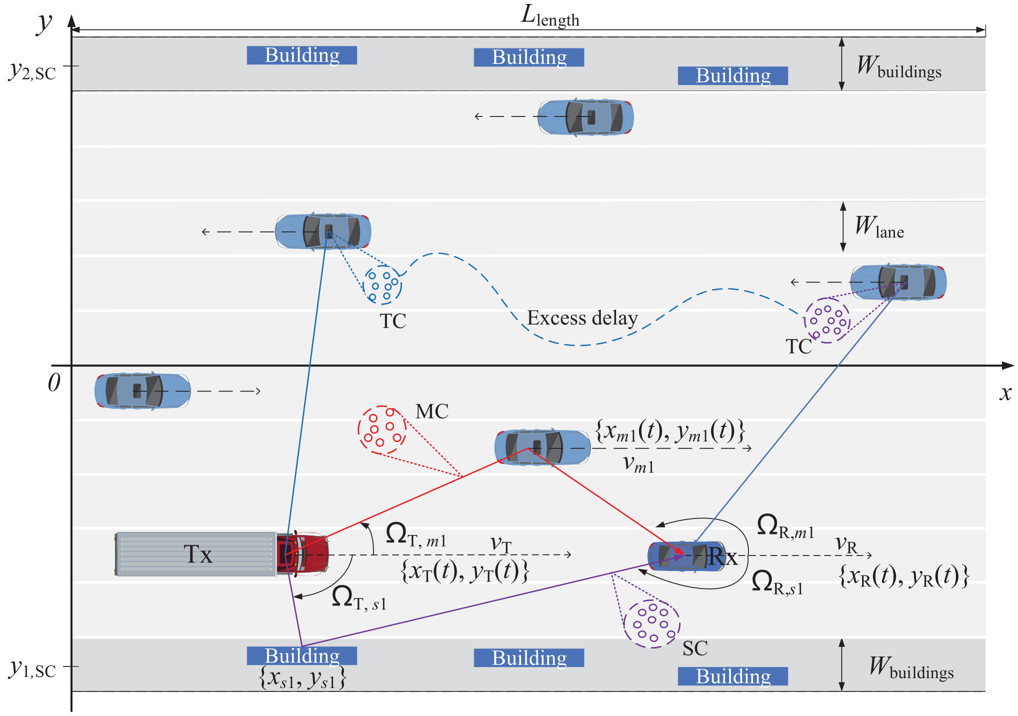

Fig. 7. Geometry map of the V2V channel model. A time-varying Tx, with coordinates $\{x_{\mathrm{T}}(t), y_{\mathrm{T}}(t)\}$, is moving at a speed of v_{T}. The Tx truck moves in the direction of the x-axis and communicates with the Rx that has the coordinates $\{x_{\mathrm{R}}(t), y_{\mathrm{R}}(t)\}$. The Rx car moves at a speed of v_{R} and travels in the direction of the x-axis on a street with the length of L_{Length}. Two types of scatterers are presented: (a) *static discrete* with coordinates $\{x_{s_i}, y_{s_i}\}$, i.e., buildings; and (b) *mobile discrete* with coordinates $\{x_{m_i}(t), y_{m_i}(t)\}$ and velocity v_{m_i}, i.e., other vehicles. The geometric relations between Tx, Rx, and static/mobile scatter are also given.

is modeled as time-variant; as such, we can thus acquire the channel components for each spatial subchannel of the MIMO channel by summarizing the whole channel using (3) at each antenna element.

Both the T2C and T2T measurement campaigns were conducted in the same freeway; however, the Rx was mounted on a truck instead of a car. Therefore, we use the same model structure in both the T2C and T2T, but changed only the model parameters. Note that we determined the speeds of the Tx/Rx in the T2C and T2T measurement campaigns from the measurement video and GPS data; thus, they will be different for the T2C and T2T.

In the single-bounce reflection propagation, the AoD and AoA of the cluster center are determined according to the geometric relationships among the physical positions of the Tx, Rx, and IOs, whereas the delay is determined according to the propagation distance. These are presented as MC and SC in Fig. 7. We determine the cluster center of the LC using similar methods, but use only the Tx and Rx without any other IOs. Note that there is no LC in the T2T channels because the container of the truck blocks the LC. In our model, the propagation involving a multi-bounce reflection, the first IO, and the last IO are randomly selected from the IOs. The AoD and AoA of the TC's center are thus decided based on the physical positions of the Tx, Rx, and first/last IOs. In addition, the delay of each TC's center is determined based on the propagation distance among the Tx-first IO and the Rx-last IO, in addition to the randomly generated excess delay (shown as TC in Fig. 7).

According to the cluster categories introduced above, (3) can be rewritten as

$$
\begin{aligned}
h_{\mathrm{sp}}(t,\tau,\Omega_R,\Omega_T) &= \sum_{l=1}^{L_{\mathrm{LC}}} h_{\mathrm{LC}}(t,\tau_l,\Omega_{R,l},\Omega_{T,l}) \\
&\quad + \sum_{n=1}^{N_{\mathrm{MC}}}\sum_{l=1}^{L_{n_{\mathrm{M}}}} h_{\mathrm{MC}}(t,\tau_{n,l},\Omega_{R,n,l},\Omega_{T,n,l}) \\
&\quad + \sum_{n=1}^{N_{\mathrm{SC}}}\sum_{l=1}^{L_{n_{\mathrm{S}}}} h_{\mathrm{SC}}(t,\tau_{n,l},\Omega_{R,n,l},\Omega_{T,n,l}) \\
&\quad + \sum_{n=1}^{N_{\mathrm{TC}}}\sum_{l=1}^{L_{n_{\mathrm{T}}}} h_{\mathrm{TC}}(t,\tau_{n,l},\Omega_{R,n,l},\Omega_{T,n,l})
\end{aligned}
\tag{4}
$$

where L_{LC} is the total number of the paths in the LC, similarly, $L_{n_{\mathrm{S}}}$ and N_{SC} are the paths in the n_{S}th SC and the total number of SCs, respectively. Likewise, N_{TC} and N_{MC} are the total number of TCs and MCs, respectively, whereas $L_{n_{\mathrm{T}}}$ and $L_{n_{\mathrm{M}}}$ are the total number of paths in the n_{T}th TC and the n_{M}th MC, respectively.

B. Scatterer Model

We have previously mentioned that the IOs in Fig. 7 are reconstructed based on the measurement environment; thus, the IO distributions are also modeled based on the physical environment. The mobile IOs are modeled as time-varying discretes and then randomly placed in a lane with fixed y-coordinates, which is at the center of each lane. In other

TABLE II
ENVIRONMENT PARAMETERS

Parameter	Part I	Part II
L_{length}	986 m	892 m
$W_{\text{buildings}}$	3 m	3 m
N_{lane}	5	5
W_{lane}	3 m	3 m
$y_{1,\text{SC}}$	16.5 m	-16.5 m
$y_{2,\text{SC}}$	16.5 m	16.5 m
χ_{SC}	0.005	0.004
χ_{MC}	0.01	0.02
D_{SCvr}	54.29 m	54.29 m
D_{MCvr}	22.27 m	22.27 m
D_p	8 m	8 m

words, each vehicle is moving along its own lane. The initial x-coordinates of each vehicle are also modeled as a continuous uniform distributions ($x_m \sim \mathcal{U}[x_{\min}, x_{\max}]$), with a certain density by the side of the x-coordinate. After initializing the simulation, each IO, Rx, and Tx are moving independently with their own time-varying speeds, $\mathbf{v}_m$, $\mathbf{v}_{\text{R}}$, and $\mathbf{v}_{\text{T}}$. Based on the initial position, velocity, and simulation time, we can derive the coordinates of each IO, Rx, and Tx.

Particularly, the static IOs' x-coordinates are modeled as a continuous uniform distribution along the length of freeway ($x_{\text{sc}} \sim \mathcal{U}[x_{\min}, x_{\max}]$), where $x_{\min}$ and $x_{\max}$ are the x-coordinates of the beginning and the end of the freeway, respectively. Similar to the vehicles, the density of the static IOs (χ_{SC}) is a constant by the side of x-coordinate. Moreover, the static IOs can be set on both sides of the freeway, and the y-coordinates of the static IOs are thus modeled as zero-mean Truncated Gaussian distributions ($y_{\text{SC}} \sim \mathcal{N}(y_{2,\text{SC}}, \sigma_{\text{SC}}, y_{2,\text{sc}} - W_{\text{buildings}}/2, y_{2,\text{sc}} + W_{\text{buildings}}/2)$ and $y_{\text{SC}} \sim \mathcal{N}(y_{1,\text{SC}}, \sigma_{\text{SC}}, y_{1,\text{sc}} - W_{\text{buildings}}/2, y_{1,\text{sc}} + W_{\text{buildings}}/2)$). We place a minimum space D_p on all IOs, Rx, and Tx to avoid generating IOs that are too close to each other. In another words, the IOs will be regenerated if it falls into other IOs'/Tx's/Rx's protection space.

We also adopt here the visibility region (VR), which has been defined in the COST 259 [70], [71] and used in the COST 2100 [72] and our previous C2C model [53]. The general idea in setting the VR is that only those IOs located in the VR regions of the Tx/Rx are involved in the propagation progress and cause single/multi-bounce reflections.[2] The details of this VR are explained in [53]. The VR of the static and mobile IOs, i.e., $D_{\text{SVR}}/D_{\text{MVR}}$, are extracted from the measurement data.

Table II presents the environment parameters, including those of the road for the model parameterization, i.e., *Part I*, and of another part of the road for the model verification, i.e., *Part II*. To implement the model for different freeway scenarios, we suggest setting the environment parameters according to the environment of interest.

[2]Assuming there is no blockage between the Tx/Rx and IOs.

TABLE III
INTERCLUSTER PARAMETERS

Parameter		$P(d_{\text{ref}})$	γ	X_δ	d_{cor}	d_{ref}
T2C	LC	33.65	1.97	4.95	40.52 m	1 m
	MC	47.56	1.93	5.65	34.36 m	1 m
	SC	55.23	2.84	3.64	24.19 m	1 m
	TC	56.84	1.53	6.16	39.54 m	1 m
T2T	MC	39.53	2.20	4.94	33.56 m	1 m
	SC	44.93	2.68	3.56	24.02 m	1 m
	TC	49.46	1.41	6.01	39.38 m	1 m

C. Cluster Structure

As a hybrid IS-GBSM, we model the channels in two steps. First, the channel characteristics of the cluster centers are modeled, e.g., inter cluster channel characteristics, followed by the MPCs in every cluster, i.e., intracluster channel properties. In this case, each IO (within the VR region) in the propagation environment can generate an SC/MC, with several MPCs following the intracluster properties. This is confirmed in both the T2T and T2C measurement data sets. The inter/intracluster parameters in each type of cluster, i.e., LC, MC, SC, and TC, are individually estimated by utilizing the nonlinear LS regression approach. Furthermore, as shown in our previous work [53], the log-distance weighted fitting can "equalize" the impact of the different amount of sampling data points on fitting parameters. Hence, we also apply this in this paper to extract the appropriate parameters.

1) Intercluster Parameters: mainly contains the number of clusters, delay, cluster power, AoD, and AoA of every cluster center. As illustrated in Section IV-B, the AoA and AoD are determined based on the geometrical relationships among the Tx, Rx, and IOs, whereas the delay of each cluster center can be derived according to the propagation distance. Next, the total cluster power (in dB) is modeled by using the well known Log-distance model [12]:

$$PL = P(d_{\text{ref}}) + 10 \cdot \gamma \cdot \log\left(\frac{d}{d_{\text{ref}}}\right) + X_\delta \tag{5}$$

where $PL(d_{\text{ref}})$ is the intercept cost of pathloss at reference distance d_{ref} (which is set to 1 m in this paper). The parameter γ represents the pathloss coefficient that quantifies the power fading changes along with the propagation distance, and X_δ represent the effect of the shadowing, which is modeled as a zero-mean Gaussian distributed random variable. Furthermore, the correlation distance of the shadowing (d_{cor}) is also modeled based on the widely used Gudmundson model.

Table III summarizes the intercluster parameters extracted from the T2C and T2T channel measurements.

2) Intracluster Parameters: mainly include the MPC properties inside the clusters. The main Intracluster parameters includes:

- **Number of MPCs within each cluster**[3]: In each cluster, the total number of MPCs L is modeled as a Poisson

[3]Parameter within each cluster indicates the intracluster parameter.

distribution:

$$f(L = k; \lambda_L) = \frac{e^{-\lambda_L}\lambda_L^k}{k!} \tag{6}$$

where parameter λ_L is the distribution coefficient.

- **Delay offset within each cluster**: In each cluster, the cluster center is determined as the MPC that has the maximum amplitude; in another word, the delay center of the cluster is the delay of the cluster center (the MPC with maximum amplitude). The delay offset is defined as the difference value between the delay center and the delay of the other MPCs. We model the delay offset for the rest of the MPCs and delay center based on the truncated Gaussian distribution:

$$f(\Delta\tau; \mu_{\Delta\tau}, \sigma_{\Delta\tau}, \tau_{\min}, \tau_{\max}) = \frac{\frac{1}{\sigma_{\Delta\tau}}\psi\left(\frac{\Delta\tau-\mu_{\Delta\tau}}{\sigma_{\Delta\tau}}\right)}{\Psi\left(\frac{\tau_{\max}-\mu_{\Delta\tau}}{\sigma_{\Delta\tau}}\right) - \Psi\left(\frac{\tau_{\min}-\mu_{\Delta\tau}}{\sigma_{\Delta\tau}}\right)} \tag{7}$$

with the range of $[\tau_{\min}, \tau_{\max}]$. The parameter ψ is the normal Gaussian distribution coefficient, with unit variance and zero mean:

$$\psi(x) = \frac{1}{\sqrt{2\pi}}e^{-\frac{1}{2}x^2} \tag{8}$$

where $\Psi(\cdot)$ is cumulative distribution function (CDF) of $\psi(\cdot)$.

- **Angular offset within each cluster**: Similar to the delay center, the angular center is defined as the AoD and AoA of the cluster center. Such that, the AoA and AoD offset between the angular center and the remaining MPCs are modeled as the widely used zero-mean Laplace distribution:

$$f(\Delta\omega; b_{\Delta\omega}) = \frac{1}{2b_{\Delta\omega}}e^{-\frac{|\Delta\omega|}{b_{\Delta\omega}}}. \tag{9}$$

- **Amplitude of the MPCs within each cluster**: In each cluster, the total cluster power (α_{cluster}) is computed according to the pathloss calculated by (5) and corresponding propagation distance, which is determined by the geometrical map. From the measurement data, we find that the MPC amplitude varies according to its position in the cluster. This indicates that the amplitude of each MPC is related to its angular offset and delay offset. Hence, we model the normalized angle delay power spectrum of each cluster as the product of a two-sided exponential function and two zero-mean Laplace functions (of delay, AoD and AoA offset). The power allocation weight factor at each angle is calculated as

$$w_{\alpha_{l,n}}(\Delta\tau_{l,n}, \Delta\omega_{\mathrm{R},l,n}, \Delta\omega_{\mathrm{T},l,n}) = e^{b_{\Delta\tau_{l,n}}\Delta\tau}e^{-\frac{|\Delta\omega_{\mathrm{R},l,n}|}{b_{\alpha,\mathrm{R}}}}e^{-\frac{|\Delta\omega_{\mathrm{T},l,n}|}{b_{\alpha,\mathrm{T}}}} \tag{10}$$

where $\Delta\tau_{l,n}$, $\Delta\omega_{\mathrm{R},l,n}$, and $\Delta\omega_{\mathrm{T},l,n}$ are the generated delay, AoA offset, and AoA offset of the lth MPC in the nth cluster, respectively, and $b_{\Delta\tau_{l,n}}$ is determined based on $\Delta\tau_{l,n}$:

$$b_{\Delta\tau_{l,n}} = \begin{cases} b_{\Delta\tau_1} & \Delta\tau_{l,n} \geq 0 \\ b_{\Delta\tau_2} & \Delta\tau_{l,n} < 0. \end{cases} \tag{11}$$

Such that, each MPC power in all cluster is allocated according to the weight factor w_{α_l}. The all set of intracluster parameters is given in Table IV.

Based on the data processing results, we can individually extract the above intracluster parameters of the LC, MC, SC, and TC. Fig. 8 shows the intracluster parameter fitting results of the LC: Fig. 8(a) shows the CDF of the number of MPCs within each clusters, which is fitted by the Poisson distribution; (b) shows the CDF of the delay offset within each clusters, which is fitted by the truncated Gaussian distribution; whereas Fig. 8(c) and (d) show the probability density function (PDF) of the AoD and AoA offset which are fitted by using the zero-mean Laplace distribution. All the distribution coefficients are provided in Table IV.

Similar to LC, the intracluster parameters of MC can be acquired using the same method, as given in Figs. 9(a)–(d); likewise, the intracluster parameters of SC can be obtained through similar procedures. Unlike the MC and SC, the propagation progress of the multi-bounce reflection is very difficult to reconstruct, as discussed in Section III-B, and we thus model it as TCs, as illustrated in Fig. 7. We compute the excess delay by using TC delay subtract LOS delay, which is consistent with the TC model in [53]. The CDFs of the excess delay and delay offset, MPC number are given in Fig. 10.

D. DMC

The DMC is considered to follow a zero-mean complex Gaussian process. Note that the DMCs are jointly modeled with noise. Its shape, as a delay function, is an exponentially decaying function plus a constant. The constant value can then be ascribed to noise, whereas the exponentially decaying function is ascribed to the DMCs [60]. The model assumes the DMC process is only correlated in frequency, where the frequency domain correlation matrix is a Toeplitz matrix [61], and its power delay profile (PDP) follows a single exponential decay model:

$$\Psi(\tau) = \begin{cases} 0 & \tau < \tau_d \\ \frac{1}{2}\alpha_1 & \tau = \tau_d \\ \alpha_1 e^{-\beta_d(\tau-\tau_d)} & \tau > \tau_d. \end{cases} \tag{12}$$

The β_d coefficient is the decay coefficient element and modeled by the log-normal distribution:

$$f(\beta_d; \mu_{\beta_d}, \sigma_{\beta_d}) = \frac{1}{\beta_d\sigma_{\beta_d}\sqrt{2\pi}}e^{-(\ln\beta_d-\mu_{\beta_d})^2/2\sigma_{\beta_d}^2} \tag{13}$$

where α_1 represents the peak power, and τ_d represents the starting delay modeled by the Poisson distribution $f(\tau_d; \lambda_{\tau_d})$. The distibution coefficients are provied in Table IV.

The coefficient α_1 is set to 10% power of the whole channels, which conforms to the channel measurements. Besides, we have modeled DMCs as spatially independent in RiMAX; thus, they are modeled as uniformly allocated in angular domain, $\Omega_{\text{dmc}} \sim \mathcal{U}[-\pi, \pi]$. All the parameters are given in Table IV, while Ref. [60] presents a more comprehensive argument of the DMC model. Some other papers, e.g., [62],

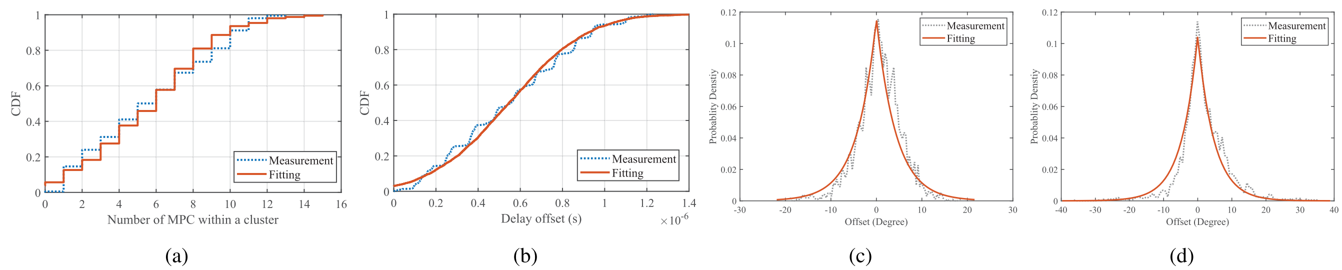

Fig. 8. Intracluster parameters for LC. (a) CDF of the amount of MPCs within clusters with the Poisson distribution fitting results; (b) CDF of delay offset with the Truncated Gaussian distribution fitting results; (c) PDF of AoA offset distribution with the Laplace distribution fitting; and (d) PDF of AoD offset distribution with the Laplace distribution fitting.

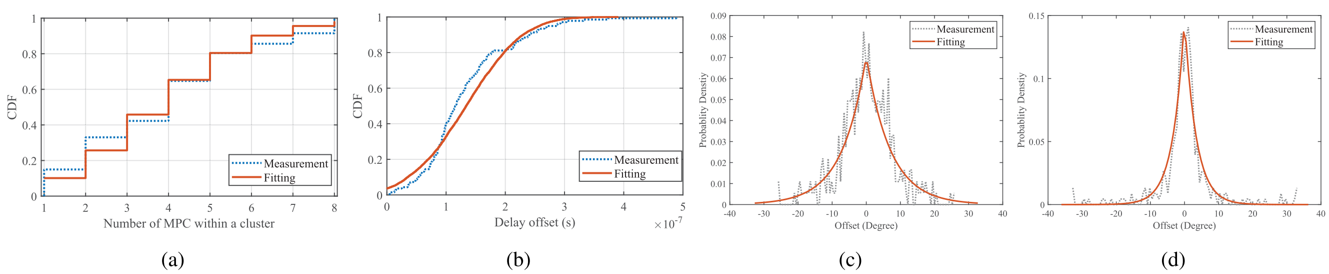

Fig. 9. Intracluster parameters for MC. (a) CDF of the amount of MPCs within clusters with the Poisson distribution fitting results; (b) CDF of delay offset with the Truncated Gaussian distribution fitting results; (c) PDF of AoA offset distribution with the Laplace distribution fitting; and (d) PDF of AoD offset distribution with the Laplace distribution fitting.

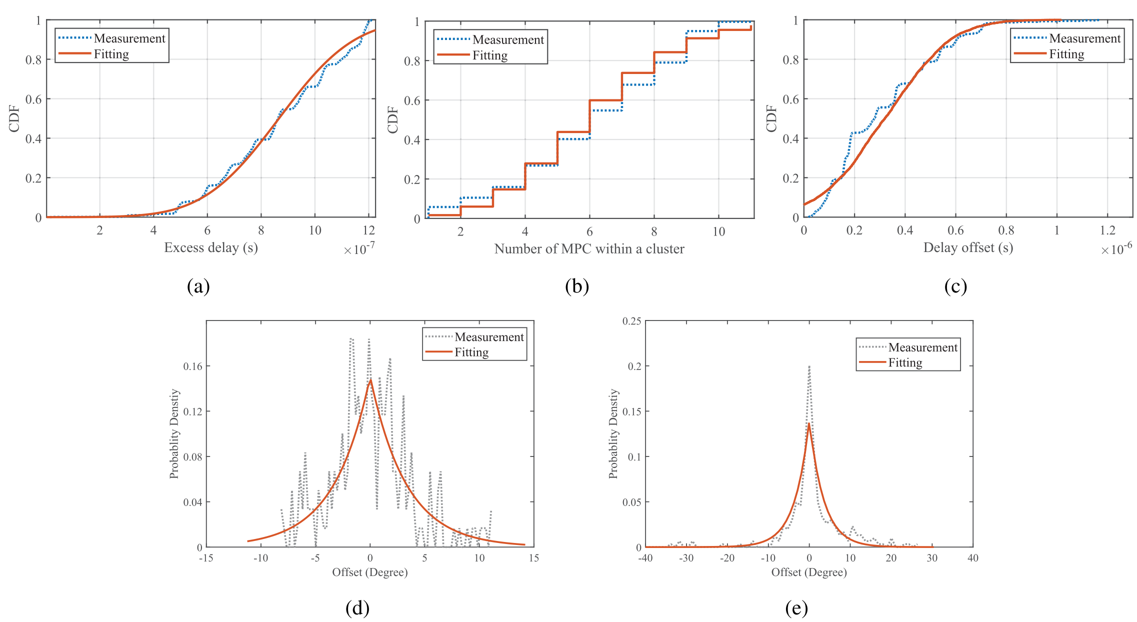

Fig. 10. Intracluster parameters for TC. (a) CDF of TC excess delay with truncated Gaussian distribution; (b) CDF of the amount of MPCs within clusters with Poisson distribution fitting results; (c) CDF of the delay offset with the Truncated Gaussian distribution fitting results; (d) PDF of AoA offset with the Laplace distribution fitting; and (e) PDF of AoD offset distribution with the Laplace distribution fitting.

also provide a different distribution of the diffuse scatterers on highways, namely, along the sides of the highway. This was motivated by the specific structure of the highway considered in these studies, which had vegetation on the sides that act as diffuse scatterers. In our setup, we consider the structures on the side of the highway as noise-reduction walls, which tend to have a more specular reflection. Thus, the DMC in our case can be seen as explaining any mismatch between the specular model and the measurement results, thereby making an angularly uniform distribution a reasonable approximation. However, we note that different distributions might also be applicable depending on the geometry of the highway.

The implementation of the overall model is the same as that in the C2C model in [53]; to avoid duplication, we refer the reader to that paper for the step-by-step application recipe.

V. Model Validation

In this part, we validate the T2C and T2T model accuracy through the delay and angular spread of the data generated by the proposed models and collected from the measurement.

TABLE IV
INTRACLUSTER PARAMETERS

Cluster Types	Parameter	Value		
		Parameter	T2C	T2T
LS	Number of MPCs	λ_L	5.12	/
	Delay offset (s)	$\mu_{\Delta\tau}$	5.51×10^{-7}	/
		$\sigma_{\Delta\tau}$	2.92×10^{-7}	/
	AoA offset (°)	$b_{\Delta\omega}$	4.58	/
	AoD offset (°)	$b_{\Delta\omega}$	4.58	/
	Amplitude fading factor	$b_{\alpha,\mathrm{R}}$	0.19	/
		$b_{\alpha,\mathrm{T}}$	0.10	/
		$b_{\Delta\tau_1}$	-0.0023	/
		$b_{\Delta\tau_2}$	inf	/
		a	0.69	/
MC	Number of MPCs	λ_L	3.87	3.23
	Delay offset (s)	$\mu_{\Delta\tau}$	1.33×10^{-7}	1.63×10^{-7}
		$\sigma_{\Delta\tau}$	7.71×10^{-8}	7.83×10^{-8}
	AOA offset (°)	$b_{\Delta\omega_\mathrm{R}}$	4.58	4.01
	AOD offset (°)	$b_{\Delta\omega_\mathrm{T}}$	4.58	4.58
	Amplitude fading factor	$b_{\alpha,\mathrm{R}}$	0.30	0.29
		$b_{\alpha,\mathrm{T}}$	0.22	0.26
		$b_{\Delta\tau_1}$	-0.0024	-0.0021
		$b_{\Delta\tau_2}$	0.0096	0.0095
		a	0.70	0.70
SC	Number of MPCs	λ_L	2.45	2.11
	Delay offset (s)	$\mu_{\Delta\tau}$	3.53×10^{-7}	3.63×10^{-7}
		$\sigma_{\Delta\tau}$	1.74×10^{-7}	1.24×10^{-7}
	AOA offset (°)	$b_{\Delta\omega_\mathrm{R}}$	5.73	5.16
	AOD offset (°)	$b_{\Delta\omega_\mathrm{T}}$	2.87	4.01
	Amplitude fading factor	$b_{\alpha,\mathrm{R}}$	0.48	0.50
		$b_{\alpha,\mathrm{T}}$	0.32	0.32
		$b_{\Delta\tau_1}$	-0.0018	-0.0028
		$b_{\Delta\tau_2}$	0.0077	0.0078
		a	0.65	0.65
TC	Number of MPCs	μ_L	6.05	xxx
	Excess Delay of TC-center (s)	μ_Ω	8.66×10^{-7}	87.0×10^{-8}
		σ_Ω	2.21×10^{-7}	2.20×10^{-7}
	Delay offset (s)	$\mu_{\Delta\tau}$	3.18×10^{-7}	3.12×10^{-7}
		$\sigma_{\Delta\tau}$	2.07×10^{-7}	2.06×10^{-7}
	AOA offset (°)	$b_{\Delta\omega_\mathrm{R}}$	3.44	3.44
	AOD offset (°)	$b_{\Delta\omega_\mathrm{T}}$	3.44	2.87
	Amplitude fading factor	$b_{\alpha,\mathrm{R}}$	0.50	0.49
		$b_{\alpha,\mathrm{T}}$	0.54	0.56
		$b_{\Delta\tau_1}$	-0.0017	-0.0020
		$b_{\Delta\tau_2}$	0.0065	0.0059
		a	0.66	0.66
DMC	Starting delay	λ_{τ_d}	49.13	48.83
	Decay factor	μ_{β_d}	-0.03	-0.03
		σ_{β_d}	0.28	0.30

Specifically, both models are evaluated based on the measurement data gathered from another part of the freeway and on the data used for the model parameterization.

In this work, the proposed GBSM is verified by using the RMS delay spread and the angular spreads. A total of 600 independent iterations are conducted to clear up the dependence among the random variable initiation. The RMS delay spread can be calculated as follows [12]

$$\tau_{rms}^{(t)} = \sqrt{\frac{\sum_{l=1}^{L}(\tau_l^{(t)} - \tau_m^{(t)})^2 |h_l^{(t)})|^2}{\sum_{l=1}^{L}|h_l^{(t)}|^2}} \tag{14}$$

where $\tau_m^{(t)}$ is the mean excess delay and can be expressed as

$$\tau_m^{(t)} = \frac{\sum_{l=1}^{L}\tau_l |h_l^{(t)}|^2}{\sum_{l=1}^{L}|h_l^{(t)}|^2}. \tag{15}$$

The angular spread is calculated according to the definition of Fleury [73], as follows

$$\lambda_{\mathrm{ASD/ASA}}^{(t)} = \sqrt{\frac{\sum_{l=1}^{L}|\exp(i\phi_{1/2,l}^{(t)}) - \mu_{\phi_{1/2}}^{(t)}|^2 |h_l^{(t)}|^2}{\sum_{l=1}^{L}|h_l^{(t)}|^2}} \tag{16}$$

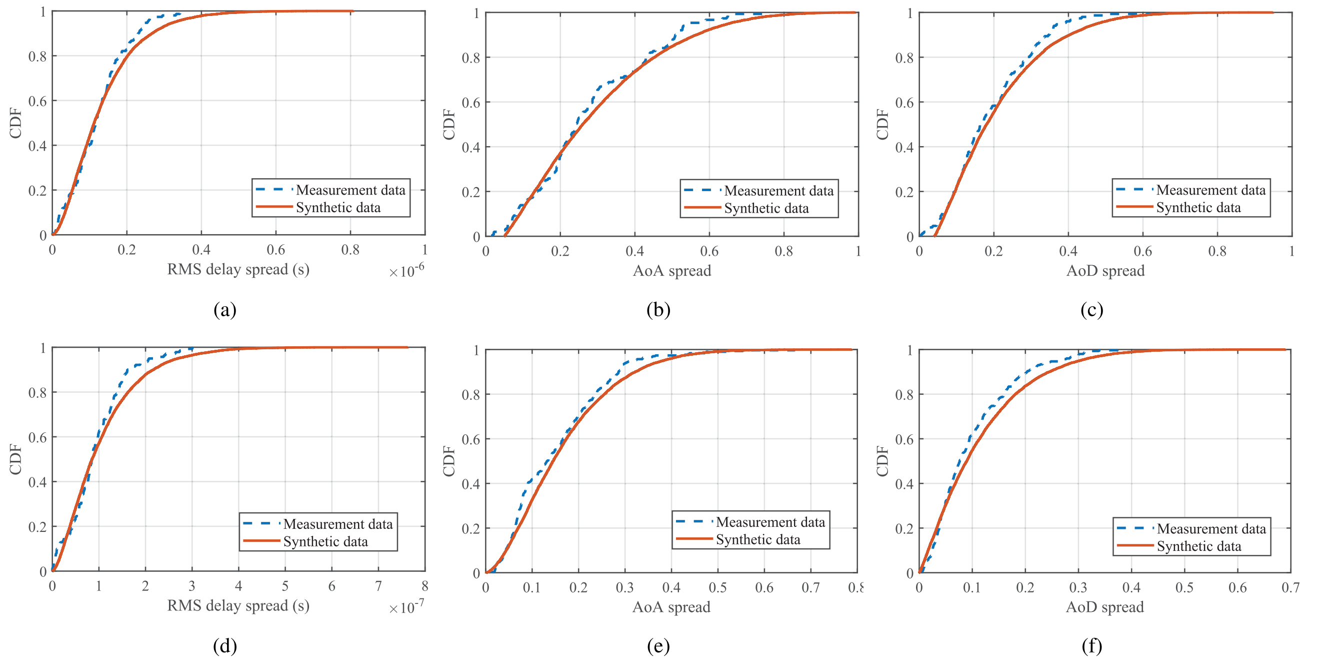

Fig. 11. Contrast between the proposed T2C model and the measured T2C channels. (a)–(c) are the contrast among synthetic data and measurement data for model parameterizations, where (d)–(e) are the contrast among synthetic data and measurement data collected from another part of the freeway.

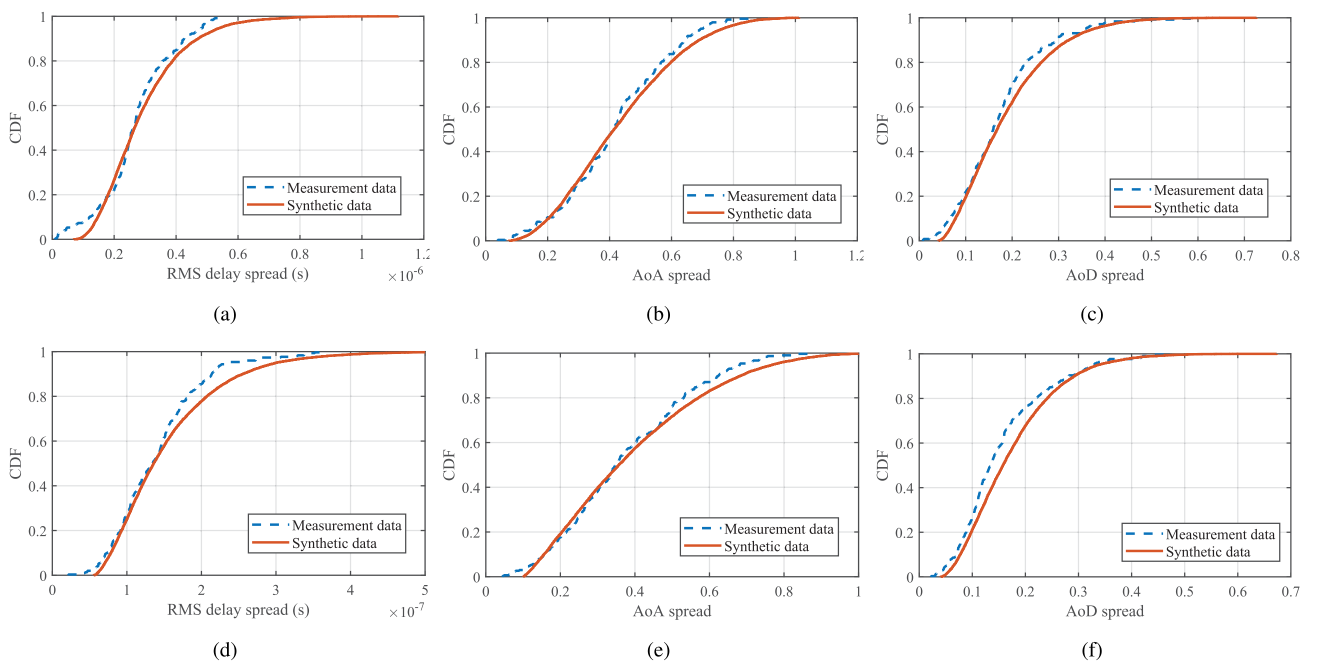

Fig. 12. Comparison between the proposed T2T model and the measured T2T channels. (a)–(c) are the comparison between the composed data and the measurement data for model parameterizations, where (d)–(e) are the comparison betweeen the synthetic data and the measurement data collected from another part of the freeway.

where the $\mu^{(t)}_{\phi_{1/2}}$ is the mean direction of the power angular spectrum. This, in turn, can be calculated as:

$$\mu^{(t)}_{\phi_{1/2}} = \frac{\sum_{l=1}^{L} \exp\left(i\phi^{(t)}_{1/2,l}\right)|h^{(t)}_l|^2}{\sum_{l=1}^{L} |h^{(t)}_l|^2}. \tag{17}$$

Fig. 11 compares the CDF of the RMS delay spread and the CDF of the angular spread of arrival/departure of the composed data generated by the proposed T2C models and the measured T2C channels. Particularly, Figs. 11(a)–(c) compare the synthetic data with the measurement data for the model parametrizations (Part I in Fig. 2(a)[4].), whereas Figs. 11(d)–(e) compare the synthetic data with the measurement data that measured from another part of the freeway (Part II in Fig. 2(a)[5]). In Fig. 12 the CDF of the angular spread and the RMS delay spread of the measured T2T models and the

[4]Contains ten MCs and ten SCs according to the environment parameters

[5]Contains seventeen MCs and seven SCs according to the environment parameters

measured T2T model are compared similarly. The physical environment parameters of both Parts I and II are given in Table II. Note that for the simulations of Part I and Part II, we modify only the physical environment parameters in accordance with the measurement, whereas the model parameters in Table III and Table IV remain the same. It can be found from the results that the synthetic data of both T2C and T2T channels match the corresponding measurement data very well. This indicates that the proposed T2C and T2T models achieve good model accuracy and can be flexibly extended to similar scenarios by modifying the environment parameters in Table II, without additional measurements.

VI. Conclusion

In this paper, a cluster-based T2X MIMO channel model has been proposed, which is proved that can characterize the properties of the wireless channel and maintaining the simplicity of the model. Specifically, the model parameterization is based on the extensive measurement data that had been collected from a freeway environment. We have categorized the MPCs into five groups according to the observations from the measurement campaign: LC, MC, SC, TC, and DMC. Next, each type of cluster has been characterized individually, and the model parameters has been extracted from the channel measurement data by conducting the RiMAX method. Then, the completed model parameterization has been provided. Eventually, we have simulated the model and compared the simulation results with the measurement data. The results show great agreement in terms of the angular spread and the RMS delay spread. Then, the model has been validated by comparing it with the channel measurement data collected from another part of the freeway different from the one for model parameterization. This then verifies that this model could be productively expanded to similar freeway scenarios. Accordingly, we conclude that the proposed model can accurately reconstruct the measured MIMO V2V channel according to the matched two second-order statistics; hence, it could help in emulating wireless V2V systems in the future.

References

[1] A. F. Molisch and F. Tufvesson, "Propagation channel models for next-generation wireless communications systems," *IEICE Trans. Commun.*, vol. E97.B, no. 10, pp. 2022–2034, 2014.

[2] C.-X. Wang, J. Bian, J. Sun, W. Zhang, and M. Zhang, "A survey of 5G channel measurements and models," *IEEE Commun. Surveys Tuts.*, vol. 20, no. 4, pp. 3142–3168, 4th Quart., 2018.

[3] C.-X. Wang, M. D. Renzo, S. Stanczak, S. Wang, and E. G. Larsson, "Artificial intelligence enabled wireless networking for 5G and beyond: Recent advances and future challenges," *IEEE Wireless Commun.*, vol. 27, no. 1, pp. 16–23, Feb. 2020.

[4] L. Lei, Z. Zhong, C. Lin, and X. Shen, "Operator controlled device-to-device communications in LTE-advanced networks," *IEEE Wireless Commun.*, vol. 19, no. 3, pp. 96–104, Jun. 2012.

[5] S. Chen, J. Hu, Y. Shi, and L. Zhao, "LTE-V: A TD-LTE-based V2X solution for future vehicular network," *IEEE Internet Things J.*, vol. 3, no. 6, pp. 997–1005, Dec. 2016.

[6] D. Jiang and L. Delgrossi, "IEEE 802.11 P: Towards an international standard for wireless access in vehicular environments," in *Proc. IEEE Veh. Technol. Conf. (VTC Spring)*, May 2008, pp. 2036–2040.

[7] G. Naik, B. Choudhury, and J.-M. Park, "IEEE 802.11bd & 5G NR V2X: Evolution of radio access technologies for V2X communications," *IEEE Access*, vol. 7, pp. 70169–70184, 2019.

[8] C. X. Wang, J. Huang, H. Wang, X. Gao, X. You, and Y. Hao, "6G wireless channel measurements and models: Trends and challenges," *IEEE Veh. Technol. Mag.*, vol. 15, no. 4, pp. 22–32, Dec. 2020.

[9] S. Wu, C.-X. Wang, E.-H.-M. Aggoune, M. M. Alwakeel, and X. You, "A general 3-D non-stationary 5G wireless channel model," *IEEE Trans. Commun.*, vol. 66, no. 7, pp. 3065–3078, Jul. 2018.

[10] X.-H. You *et al.*, "Towards 6G wireless communication networks: Vision, enabling technologies, and new paradigm shifts," *Sci. China Inf. Sci.*, vol. 64, no. 1, pp. 1–74, Jan. 2021.

[11] S. Chen *et al.*, "Vehicle-to-everything (v2x) services supported by LTE-based systems and 5G," *IEEE Commun. Standards Mag.*, vol. 1, no. 2, pp. 70–76, Jun. 2017.

[12] A. F. Molisch, *Wireless Communications*, vol. 34. Hoboken, NJ, USA: Wiley, Feb. 2012.

[13] A. F. Molisch, F. Tufvesson, J. Kåredal, and C. F. Mecklenbräuker, "A survey on vehicle-to-vehicle propagation channels," *IEEE Commun. Mag.*, vol. 16, no. 6, pp. 12–22, Dec. 2009.

[14] G. Acosta and M. A. Ingram, "Model development for the wideband expressway vehicle-to-vehicle 2.4 GHz channel," in *Proc. IEEE WCNC*, Las Vegas, NV, USA, vol. 3, Apr. 2006, pp. 1283–1288.

[15] I. Sen and D. W. Matolak, "Vehicle–vehicle channel models for the 5-GHz band," *IEEE Trans. Intell. Transp. Syst.*, vol. 9, no. 2, pp. 235–245, Jun. 2008.

[16] J. Maurer, T. Fugen, and W. Wiesbeck, "Narrow-band measurement and analysis of the inter-vehicle transmission channel at 5.2 GHz," in *Proc. IEEE VTC-Spring*, Birmingham, AL, USA, May 2002, pp. 1274–1278.

[17] O. Renaudin, V.-M. Kolmonen, P. Vainikainen, and C. Oestges, "Wide-band measurement-based modeling of inter-vehicle channels in the 5-GHz band," *IEEE Trans. Veh. Technol.*, vol. 62, no. 8, pp. 3531–3540, Oct. 2013.

[18] L. Cheng, B. Henty, F. Bai, and D. D. Stancil, "Doppler spread and coherence time of rural and highway vehicle-to-vehicle channels at 5.9 GHz," in *Proc. IEEE Global Telecommun. Conf. (GLOBECOM)*, New Orleans, LO, USA, Nov. 2008, pp. 1–6.

[19] L. Cheng, B. E. Henty, F. Bai, and D. D. Stancil, "Highway and rural propagation channel modeling for vehicle-to-vehicle communications at 5.9 GHz," in *Proc. IEEE Antennas Propag. Soc. Int. Symp.*, San Diego, CA, USA, Jul. 2008, pp. 1–4.

[20] L. Cheng, B. E. Henty, D. D. Stancil, F. Bai, and P. Mudalige, "Mobile vehicle-to-vehicle narrow-band channel measurement and characterization of the 5.9 GHz dedicated short range communication (DSRC) frequency band," *IEEE J. Sel. Areas Commun.*, vol. 25, no. 8, pp. 1501–1516, Oct. 2007.

[21] M. Boban, J. Barros, and O. K. Tonguz, "Geometry-based vehicle-to-vehicle channel modeling for large-scale simulation," *IEEE Trans. Veh. Technol.*, vol. 63, no. 9, pp. 4146–4164, Nov. 2014.

[22] M. G. Nilsson, D. Vlastaras, T. Abbas, B. Bergqvist, and F. Tufvesson, "On multilink shadowing effects in measured V2V channels on highway," in *Proc. 9th Eur. Conf. Antennas Propag. (EuCAP)*, Apr. 2015, pp. 1–5.

[23] M. G. Nilsson, C. Gustafson, T. Abbas, and F. Tufvesson, "A measurement-based multilink shadowing model for V2 V network simulations of highway scenarios," *IEEE Trans. Veh. Technol.*, vol. 66, no. 10, pp. 8632–8643, Oct. 2017.

[24] T. Fan, W. Chen, C. Li, X. Shu, and F. Chang, "Small scale characteristics analysis on highway V2 V channel for intelligent transportation systems," in *Proc. 5th Int. Conf. Transp. Inf. Saf. (ICTIS)*, Jul. 2019, pp. 789–793.

[25] K. Karlsson, C. Bergenhem, and E. Hedin, "Field measurements of IEEE 802.11p communication in NLOS environments for a platooning application," in *Proc. IEEE Veh. Technol. Conf. (VTC Fall)*, Sep. 2012, pp. 1–5.

[26] H. Fernandez, V. M. Rodrigo-Penarrocha, L. Rubio, and J. Reig, "Path loss characterization in vehicular environments under LOS and NLOS conditions at 5.9 GHz," in *Proc. 8th Eur. Conf. Antennas Propag. (EuCAP)*, Apr. 2014, pp. 3044–3048.

[27] J. Blumenstein *et al.*, "Measured high-resolution power-delay profiles of nonstationary vehicular millimeter wave channels," in *Proc. IEEE 29th Annu. Int. Symp. Pers., Indoor Mobile Radio Commun. (PIMRC)*, Sep. 2018, pp. 1–5.

[28] D. Vlastaras, T. Abbas, M. Nilsson, R. Whiton, M. Olbäck, and F. Tufvesson, "Impact of a truck as an obstacle on vehicle-to-vehicle communications in rural and highway scenarios," in *Proc. 6th Int. Symp. Wireless Veh. Commun. (WiVeC)*, Sep. 2014, pp. 1–6.

[29] J. Karedal, N. Czink, A. Paier, F. Tufvesson, and A. F. Molisch, "Path loss modeling for vehicle-to-vehicle communications," *IEEE Trans. Veh. Technol.*, vol. 60, no. 1, pp. 323–328, Jan. 2010.

[30] A. Paier *et al.*, "Characterization of vehicle-to-vehicle radio channels from measurements at 5.2 GHz," *Wireless Pers. Commun.*, vol. 50, no. 1, pp. 19–32, Jul. 2009.

[31] A. Paier *et al.*, "Spatial diversity and spatial correlation evaluation of measured vehicle-to-vehicle radio channels at 5.2 GHz," in *Proc. IEEE 13th Digit. Signal Process. Workshop 5th IEEE Signal Process. Educ. Workshop*, Jan. 2009, pp. 326–330.

[32] O. Renaudin, V.-M. Kolmonen, P. Vainikainen, and C. Oestges, "Car-to-car channel models based on wideband MIMO measurements at 5.3 GHz," in *Proc. ECAP*, Berlin, Germany, Mar. 2009, pp. 635–639.

[33] O. Renaudin, V.-M. Kolmonen, P. Vainikainen, and C. Oestges, "Non-stationary narrowband MIMO inter-vehicle channel characterization in the 5-GHz band," *IEEE Trans. Veh. Technol.*, vol. 59, no. 4, pp. 2007–2015, May 2010.

[34] T. Abbas, L. Bernado, A. Thiel, C. Mecklenbrauker, and F. Tufvesson, "Radio channel properties for vehicular communication: Merging lanes versus urban intersections," *IEEE Veh. Technol. Mag.*, vol. 8, no. 4, pp. 27–34, Dec. 2013.

[35] T. Abbas, L. Bernado, A. Thiel, C. F. Mecklenbrauker, and F. Tufvesson, "Measurements based channel characterization for vehicle-to-vehicle communications at merging lanes on highway," in *Proc. IEEE 5th Int. Symp. Wireless Veh. Commun. (WiVeC)*, Jun. 2013, pp. 1–5.

[36] R. He, A. F. Molisch, F. Tufvesson, Z. Zhong, B. Ai, and T. Zhang, "Vehicle-to-vehicle propagation models with large vehicle obstructions," *IEEE Trans. Intell. Transp. Syst.*, vol. 15, no. 5, pp. 2237–2248, Oct. 2014.

[37] M. Yang *et al.*, "Measurements and cluster-based modeling of vehicle-to-vehicle channels with large vehicle obstructions," *IEEE Trans. Wireless Commun.*, vol. 19, no. 9, pp. 5860–5874, Sep. 2020.

[38] M. Boban, T. T. V. Vinhoza, M. Ferreira, J. Barros, and O. K. Tonguz, "Impact of vehicles as obstacles in vehicular ad hoc networks," *IEEE J. Sel. Areas Commun.*, vol. 29, no. 1, pp. 15–28, Jan. 2010.

[39] R. Meireles, M. Boban, P. Steenkiste, O. Tonguz, and J. Barros, "Experimental study on the impact of vehicular obstructions in VANETs," in *Proc. IEEE Veh. Netw. Conf. (VNC)*, Jersey City, NJ, USA, Dec. 2010, pp. 338–345.

[40] D. Vlastaras, R. Whiton, and F. Tufvesson, "A model for power contributions from diffraction around a truck in vehicle-to-vehicle communications," in *Proc. 15th Int. Conf. ITS Telecommun. (ITST)*, May 2017, pp. 1–6.

[41] Q. Wang, D. W. Matolak, and B. Ai, "Shadowing characterization for 5-GHz vehicle-to-vehicle channels," *IEEE Trans. Veh. Technol.*, vol. 67, no. 3, pp. 1855–1866, Mar. 2018.

[42] K. Karlsson, J. Carlsson, M. Larsson, and C. Bergenhem, "Evaluation of the V2V channel and diversity potential for platooning trucks," in *Proc. EuCAP*, Davos, Switzerland, Apr. 2016, pp. 1–5.

[43] O.-Y. Kwon, R. Song, Y.-Z. Ma, and B.-S. Kim, "Integrated MIMO antennas for LTE and V2 V applications," in *Proc. URSI Asia–Pacific Radio Sci. Conf. (URSI AP-RASC)*, Aug. 2016, pp. 1057–1060.

[44] T. Fugen, J. Maurer, W. Sorgel, and W. Wiesbeck, "Characterization of multipath clusters with ray-tracing in urban MIMO propagation environments at 2 GHz," in *Proc. IEEE Antennas Propag. Soc. Int. Symp.*, Jul. 2005, pp. 410–413.

[45] M. Yang *et al.*, "A cluster-based three-dimensional channel model for vehicle-to-vehicle communications," *IEEE Trans. Veh. Technol.*, vol. 68, no. 6, pp. 5208–5220, Jun. 2019.

[46] M. Ingram, G. Acosta, and L. Dong, "Small-scale fading models for IEEE 802.11 P (WAVE/DSRC) standard," Georgia Inst. Technol., Atlanta, GA, USA, Tech. Rep. 11-06-1724, Sep. 2006. [Online]. Available: https://mentor.ieee.org/802.11/dcn/06/11-06-1724-00-000p-wave-channel-model-doc

[47] R. B. Ertel and J. H. Reed, "Angle and time of arrival statistics for circular and elliptical scattering models," *IEEE J. Sel. Areas Commun.*, vol. 17, no. 11, pp. 1829–1840, Nov. 1999.

[48] S. J. Nawaz, M. Riaz, N. M. Khan, and S. Wyne, "Temporal analysis of a 3D ellipsoid channel model for the vehicle-to-vehicle communication environments," *Wireless Pers. Commun.*, vol. 82, no. 3, pp. 1337–1350, Jun. 2015.

[49] X. Zhao, X. Liang, S. Li, and B. Ai, "Two-cylinder and multi-ring GBSSM for realizing and modeling of vehicle-to-vehicle wideband MIMO channels," *IEEE Trans. Intell. Transp. Syst.*, vol. 17, no. 10, pp. 2787–2799, Oct. 2016.

[50] A. G. Zajic, G. L. Stuber, T. G. Pratt, and S. T. Nguyen, "Wideband MIMO mobile-to-mobile channels: Geometry-based statistical modeling with experimental verification," *IEEE Trans. Veh. Technol.*, vol. 58, no. 2, pp. 517–534, Feb. 2009.

[51] C. Gustafson, K. Mahler, D. Bolin, and F. Tufvesson, "The COST IRACON geometry-based stochastic channel model for vehicle-to-vehicle communication in intersections," *IEEE Trans. Veh. Technol.*, vol. 69, no. 3, pp. 2365–2375, Mar. 2020.

[52] H. Chang *et al.*, "A novel nonstationary 6G UAV-to-Ground wireless channel model with 3-D arbitrary trajectory changes," *IEEE Internet Things J.*, vol. 8, no. 12, pp. 9865–9877, Jun. 2021.

[53] C. Huang *et al.*, "Geometry-cluster-based stochastic MIMO model for vehicle-to-vehicle communications in street canyon scenarios," *IEEE Trans. Wireless Commun.*, vol. 20, no. 2, pp. 755–770, Feb. 2021.

[54] J. Bian, C.-X. Wang, X. Gao, X. You, and M. Zhang, "A general 3D non-stationary wireless channel model for 5G and beyond," *IEEE Trans. Wireless Commun.*, vol. 20, no. 5, pp. 3211–3224, May 2021.

[55] A. F. Molisch, A. Kuchar, J. Laurila, K. Hugl, and R. Schmalenberger, "Geometry-based directional model for mobile radio channels?Principles and implementation," *Eur. Trans. Telecommun.*, vol. 14, no. 4, pp. 351–359, Jul. 2003.

[56] A. F. Molisch, "A generic model for MIMO wireless propagation channels in macro- and microcells," *IEEE Trans. Signal Process.*, vol. 52, no. 1, pp. 61–71, Jan. 2004.

[57] Q. H. Spencer, B. D. Jeffs, M. A. Jensen, and A. L. Swindlehurst, "Modeling the statistical time and angle of arrival characteristics of an indoor multipath channel," *IEEE J. Sel. Areas Commun.*, vol. 18, no. 3, pp. 347–360, Mar. 2000.

[58] R. Wang, C. U. Bas, O. Renaudin, S. Sangodoyin, U. T. Virk, and A. F. Molisch, "A real-time MIMO channel sounder for vehicle-to-vehicle propagation channel at 5.9 GHz," in *Proc. IEEE Int. Conf. Commun. (ICC)*, May 2017, pp. 1–6.

[59] B. H. Fleury, M. Tschudin, R. Heddergott, D. Dahlhaus, and K. Ingeman Pedersen, "Channel parameter estimation in mobile radio environments using the SAGE algorithm," *IEEE J. Sel. Areas Commun.*, vol. 17, no. 3, pp. 434–450, Mar. 1999.

[60] R. Wang, O. Renaudin, C. U. Bas, S. Sangodoyin, and A. F. Molisch, "High-resolution parameter estimation for time-varying double directional V2V channel," *IEEE Trans. Wireless Commun.*, vol. 16, no. 11, pp. 7264–7275, Nov. 2017.

[61] A. Richter, "Estimation of radio channel parameters: Models and algorithms," Ph.D. dissertation, Dept. Elect. Eng. Inf. Technol., Techn. Univ. Ilmenau, Ilmenau, Germany, May 2005. [Online]. Available: http://www.db-thueringen.de

[62] J. Karedal *et al.*, "A geometry-based stochastic MIMO model for vehicle-to-vehicle communications," *IEEE Trans. Wireless Commun.*, vol. 8, no. 7, pp. 3646–3657, Jul. 2009.

[63] R. Wang, O. Renaudin, C. U. Bas, S. Sangodoyin, and A. F. Molisch, "Vehicle-to-vehicle propagation channel for truck-to-truck and mixed passenger freight convoy," in *Proc. IEEE 28th Annu. Int. Symp. Pers., Indoor, Mobile Radio Commun. (PIMRC)*, Oct. 2017, pp. 1–5.

[64] C. Huang, R. He, Z. Zhong, Y.-A. Geng, Q. Li, and Z. Zhong, "A novel tracking-based multipath component clustering algorithm," *IEEE Antennas Wireless Propag. Lett.*, vol. 16, pp. 2679–2683, 2017.

[65] N. Czink *et al.*, "Tracking time-variant cluster parameters in MIMO channel measurements," in *Proc. 2nd Int. Conf. Commun. Netw. China (CHINACOM)*, Aug. 2007, pp. 1147–1151.

[66] C. Huang *et al.*, "A power-angle-spectrum based clustering and tracking algorithm for time-varying radio channels," *IEEE Trans. Veh. Technol.*, vol. 68, no. 1, pp. 291–305, Jan. 2019.

[67] N. Czink, C. Mecklenbrauker, and G. D. Galdo, "A novel automatic cluster tracking algorithm," in *Proc. IEEE 17th Int. Symp. Pers., Indoor Mobile Radio Commun.*, Helsinki, Finland, Sep. 2006, pp. 1–5.

[68] C. Huang, A. F. Molisch, Y.-A. Geng, R. He, B. Ai, and Z. Zhong, "Trajectory-joint clustering algorithm for time-varying channel modeling," *IEEE Trans. Veh. Technol.*, vol. 69, no. 1, pp. 1041–1045, Jan. 2020.

[69] H. Hofstetter, A. F. Molisch, and N. Czink, "A twin-cluster MIMO channel model," in *Proc. IEEE EuCAP*, Nov. 2006, pp. 1–8.

[70] A. F. Molisch, H. Asplund, R. Heddergott, M. Steinbauer, and T. Zwick, "The COST259 directional channel model—Part I: Overview and methodology," *IEEE Trans. Wireless Commun.*, vol. 5, no. 12, pp. 3421–3433, Dec. 2006.

[71] H. Asplund, A. A. Glazunov, A. F. Molisch, K. I. Pedersen, and M. Steinbauer, "The COST 259 directional channel model—Part II: Macrocells," *IEEE Trans. Wireless Commun.*, vol. 5, no. 12, pp. 3434–3450, Dec. 2006.

[72] L. Liu *et al.*, "The COST 2100 MIMO channel model," *IEEE Wireless Commun.*, vol. 19, no. 6, pp. 92–99, Dec. 2012.

[73] B. H. Fleury, "First- and second-order characterization of direction dispersion and space selectivity in the radio channel," *IEEE Trans. Inf. Theory*, vol. 46, no. 6, pp. 2027–2044, Sep. 2000.

Chen Huang (Member, IEEE) received the B.E. and M.S. degrees from the Chongqing University of Posts and Telecommunications (CQUPT), Chongqing, China, in 2013 and 2016, respectively, and the Ph.D. degree from Beijing Jiaotong University, Beijing, China, in 2021.

He is currently a Research Fellow with the Pervasive Communication Research Center, Purple Mountain Laboratories, Nanjing, China; and also a Post-Doctoral Researcher with the National Mobile Communications Research Laboratory, School of Information Science and Engineering, Southeast University, Nanjing. From 2018 to 2020, he has been a Visiting Scholar with the University of Southern California, Los Angeles, CA, USA; and the Université Catholique de Louvain (UCL), Louvain-la-Neuve, Belgium. He has authored/coauthored one book chapter and more than 40 journals and conference papers, as well as several patents. His research interests include channel parameters analysis and characterization, clustering and tracking, time-varying channel modeling, and applications of machine learning-based techniques on propagation channel characterization. He is selected in the Outstanding Postdoctoral Fellow Program in Jiangsu, received two times the Best Paper Award at international conferences; and serves as the Technical Program Committee (TPC) Member for VTC-full 2019.

Rui Wang (Member, IEEE) received the B.S. degree from Southeast University, Nanjing, China, in 2010, and the M.S. (Hons.) and doctorate degrees in electrical engineering from the University of Southern California, Los Angeles, CA, USA, in 2012 and 2018, respectively. He worked on massive MIMO technology for 4G/5G cellular systems at Samsung Research America, Mountain View, CA, USA. He is currently a Software Engineer at Google, Mountain View, CA, USA. His research interests include wireless channel measurements and modeling for vehicle-to-vehicle and mm-wave communication systems. He is also interested in statistical signal processing and optimization algorithms.

Cheng-Xiang Wang (Fellow, IEEE) received the B.Sc. and M.Eng. degrees in communication and information systems from Shandong University, China, in 1997 and 2000, respectively, and the Ph.D. degree in wireless communications from Aalborg University, Denmark, in 2004.

He was a Research Assistant with the Hamburg University of Technology, Hamburg, Germany, from 2000 to 2001; a Visiting Researcher with Siemens AG Mobile Phones, Munich, Germany, in 2004; and a Research Fellow with the University of Agder, Grimstad, Norway, from 2001 to 2005. He has been with Heriot-Watt University, Edinburgh, U.K., since 2005, where he was promoted to a Professor in 2011. In 2018, he joined Southeast University, Nanjing, China, as a Professor. He is also a part-time Professor with Purple Mountain Laboratories, Nanjing. He has authored four books, three book chapters, and more than 460 papers in refereed journals and conference proceedings, including 26 highly cited papers. He has also delivered 23 invited keynote speeches/talks and ten tutorials in international conferences. His current research interests include wireless channel measurements and modeling, 6G wireless communication networks, and electromagnetic information theory.

Dr. Wang is a member of the Academia Europaea (The Academy of Europe) and the European Academy of Sciences and Arts (EASA); a fellow of the Royal Society of Edinburgh (FRSE), IET, and China Institute of Communications (CIC); a Distinguished Lecturer of IEEE Communications Society in 2019 and 2020; and a Highly-Cited Researcher recognized by Clarivate Analytics from 2017 to 2020. He is currently an Executive Editorial Committee Member of the IEEE TRANSACTIONS ON WIRELESS COMMUNICATIONS. He has served as a TPC Member, the TPC chair, and the general chair for more than 80 international conferences. He received 14 Best Paper Awards from IEEE GLOBECOM 2010, IEEE ICCT 2011, ITST 2012, IEEE VTC 2013 Spring, IWCMC 2015, IWCMC 2016, IEEE/CIC ICCC 2016, WPMC 2016, WOCC 2019, IWCMC 2020, WCSP 2020, CSPS 2021, and WCSP 2021. He received the 2020–2022 "AI 2000 Most Influential Scholar Award Honorable Mention" in recognition of his outstanding and vibrant contributions in the field of the Internet of Things. He served as an Editor for over ten international journals, including the IEEE TRANSACTIONS ON WIRELESS COMMUNICATIONS from 2007 to 2009, the IEEE TRANSACTIONS ON VEHICULAR TECHNOLOGY from 2011 to 2017, and the IEEE TRANSACTIONS ON COMMUNICATIONS from 2015 to 2017. He was a Lead Guest Editor for the Special Issue on Vehicular Communications and Networks and a Guest Editor for the Special Issue on the Spectrum and Energy Efficient Design of Wireless Communication Networks and the Special Issue on Airborne Communication Networks of the IEEE JOURNAL ON SELECTED AREAS IN COMMUNICATIONS. He was also a Guest Editor for the Special Issue on Wireless Big Data of the IEEE TRANSACTIONS ON BIG DATA and is a Guest Editor for the Special Issue on Intelligent Resource Management for 5G and Beyond of the IEEE TRANSACTIONS ON COGNITIVE COMMUNICATIONS AND NETWORKING.

Pan Tang (Member, IEEE) received the B.S. degree in electrical information engineering from the South China University of Technology, Guangzhou, China, in 2013, and the Ph.D. degree in information and communication engineering from the Beijing University of Posts and Telecommunications, Beijing, China, in 2019. From 2017 to 2018, he was a Visiting Scholar with the University of Southern California. From 2019 to 2021, he was a Post-Doctoral Research Associate with the Beijing University of Posts and Telecommunications, China. He is currently an Associate Professor with the State Key Laboratory of Networking and Switching Technology, Beijing University of Posts and Telecommunications. He has authored and coauthored more than 40 papers in refereed journals and conference proceedings. His current research interests include millimeter wave, THz, and visible light channel measurements and modeling.

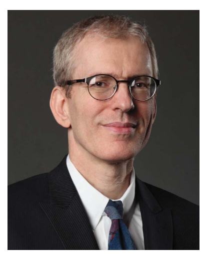

Andreas F. Molisch (Fellow, IEEE) received the degrees (Dipl.Ing. 1990, Ph.D. 1994, Habilitation 1999) from the Technical University Vienna, Austria. He spent the next ten years in industry, at FTW, AT&T (Bell) Laboratories, and Mitsubishi Electric Research Labs (where he rose to Chief Wireless Standards Architect). In 2009, he joined the University of Southern California (USC), Los Angeles, CA, USA, as a Professor, and founded the Wireless Devices and Systems (WiDeS) Group. In 2017, he was appointed to the Solomon Golomb-Andrew and Erna Viterbi Chair.

His research interests revolve around wireless propagation channels, wireless systems design, and their interaction. Recently, his main interests have been wireless channel measurement and modeling for 5G and beyond 5G systems, joint communication-caching-computation, hybrid beamforming, UWB/TOA-based localization, and novel modulation/multiple access methods. Overall, he has published five books (among them the textbook *Wireless Communications* third edition in 2022), 21 book chapters, 280 journal articles, and 370 conference papers. He is also the inventor of 70 granted (and more than ten pending) patents, and coauthor of some 70 standards contributions. His work has been cited more than 59 000 times, his H-index is >100, and he is a Clarivate Highly Cited Researcher.

Dr. Molisch has been an Editor of a number of journals and special issues, the General Chair, the Technical Program Committee Chair, or the Symposium Chair of multiple international conferences, as well as the Chairperson of various international standardization groups. He is a fellow of the National Academy of Inventors, fellow of the AAAS, fellow of the IET, an IEEE Distinguished Lecturer, and a member of the Austrian Academy of Sciences. He has received numerous awards, among them the IET Achievement Medal, the Technical Achievement Awards of IEEE Vehicular Technology Society (Evans Avant-Garde Award), and the IEEE Communications Society (Edwin Howard Armstrong Award), and the Technical Field Award of the IEEE for Communications, the Eric Sumner Award.